Arabian Journal for Science and Engineering (2018) 43:5439–5455
https://doi.org/10.1007/s13369-018-3147-9

RESEARCH ARTICLE - CIVIL ENGINEERING

Dynamic Response of Segment Lining of Overlapped Shield Tunnels Under Train-Induced Vibration Loads

Qi-xiang Yan[1] · Le-yang Song[1] · Hang Chen[1] · Wen-yu Chen[1] · Shu-qi Ma[1] · Wen-bo Yang[1]

Received: 6 December 2017 / Accepted: 4 February 2018 / Published online: 5 March 2018

Abstract
The dynamic response of the overlapped shield tunnels subjected to the train-induced vibration is studied using a nonlinear finite element software. A three-dimensional numerical model is established, and the fabricated segment linings which contain steel bars are used to simulate the shield tunnel. The interaction behaviors, i.e., tensile, shear, and bending, between segment linings are successfully captured by defining the segment lining circumference interface and the joint bolt model. The results show that the dynamic response of the segment linings of the overlapped shield tunnels is affected by the vibration loads caused by the running trains. The additional internal forces generated in the shield tunnels with the fabricated segment linings (joint interfaces are explicitly represented) are larger than those of tunnels which use homogeneous equivalent stiffness model. The opening and staggered deformation response of the joint interfaces is related to the train locations. The axial force and shear response of the bolt under the dynamic load of the train are closely associated with the opening and staggered deformation of joints. The steel spring floating slab can greatly reduce the vertical acceleration and the displacement at the arch bottom of the lower tunnel. The vertical acceleration and the displacement of the bottom arch at the L-III segment lining with the steel spring floating plates are 0.65 times and 0.78 times of the tunnels without the steel spring floating plates, respectively. This study reveals the vibration response features of the overlapped shield tunnels under the train-induced vibration loads, which will help improve the waterproofing capacity and stability of shield tunnels.

Keywords Overlapped shield tunnel · Train vibration load · Segment lining radial internal force · Joint bolts · Joint internal force · Interface deformation

1 Introduction

The urbanization population is increased dramatically in China. Most of large cities in China are developing or planning the urban subway projects to alleviate the pressure of urban traffic. At present, metro tunnels are mainly constructed by using shield tunnel method. The formation of the overlapped shield tunnels is inevitable. For instance, a total mileage of 185.65 km have been put into operation for Wuhan subway and some of the metro lines are overlapped vertically. This type of overlapped structures is prone to damage as they are subjected to the train-induced vibration loads as well as the interaction between the upper and lower tunnels. The complex loading condition could lead to opening and staggering of the segment linings of the overlapped tunnels, which would affect the waterproof performance of the tunnel structure [1–4]. Therefore, it is of great significance to study the dynamic response of the overlapped tunnel structure under the train caused vibration load, which would be helpful for the reinforcement design and for the determination of relative distance between overlapped tunnels.

Dynamic response of the tunnels under the train-induced vibration loads has now attracted considerable attentions. Lai et al. [5]analyzed the vibration response of the metro tunnel structure in terms of acceleration, velocity, displacement, and stress, for the crossing tunnel structure (CTS) of Metro Line 2 and the Yongningmen tunnel in Xi'an, China.

Clot et al. [6] used a three-dimensional dynamic model to calculate the ground-borne vibrations generated by harmonic loads which were applied on the interior floor of a double-deck circular tunnel. Xue [7] found that the spatial

✉ Shu-qi Ma
shuqima.ma@gmail.com

✉ Wen-bo Yang
397730110@qq.com

[1] Key Laboratory of Transportation Tunnel Engineering (Southwest Jiaotong University), Ministry of Education, Chengdu 610031, China

distributions of dynamic displacement, velocity, acceleration, and stresses of the rail-tunnel-foundation system are associated with time and space. Gardien and Stuit [8] presented a modular model to simulate the railway traffic-induced vibrations, and their model considered the static deflection model (3D FEM), the track model, and the propagation model. Yanet al. [9] studied the dynamic response of the tunnel linings under various vehicle speeds and rock mass properties. Real et al. [10] developed a 3D numerical FEM model of a railway tunnel to predict railway-induced vibrations, and the FEM model is validated by in situ measurements.

Effects of joints between segments on the mechanical properties of tunnel linings have also been studied. Gharehdash and Barzegar [11] compared the dynamic response of the shield tunnel buried in soft soil when the joint effects are considered and when the joint effects are not considered. Li et al. [12] studied the influences of the calking groove and the pretightening bolt on the mechanical behavior of the structure, by establishing three-dimensional solid segment and bolt model for the cast iron segment. Yan et al. [13] studied the failure behavior of joint bolts in a shield tunnel under the dynamic impacts induced by trains. In their study, a three-dimensional numerical model of a shield tunnel was established with consideration of joints between segments. Hefny and Chua [14] showed that the increase in the joint number reduces the maximum bending moment induced in the lining. However, the effects of the joint number on the maximum bending moment of the lining become insignificant once the critical joint number has been exceeded. Deng et al. [15] studied the dynamic response of the shield tunnel buried in thick soft soil under the vibration induced by a metro train. The A-B-K segments were used in his model, and the joint effects were considered. Mo et al. [16] also studied the dynamic response of a shield tunnel buried in thick soft soil with consideration of joints between segments.

In practice, the vibration loads induced by a train vary with time and, however, the above study does not consider the time-dependent vibration loads induced by the train. In addition, the interaction mechanism of the overlapped tunnels is also not accounted for. A few studies have been conducted on the dynamic response of the overlapped tunnel structure where the prefabricated segment linings are installed, with the consideration of joint bolt internal force and the joint interface deformation.

The dynamic response of the overlapped tunnel of the Wuhan Metro Line 2 (from Xunlimen station to Jiyuqiao station) and the Line 6 (from Jianghan Road station to Dazhi Road station) is numerically studied in this paper (Fig. 1). The finite element software ABAQUS [17] is used, and a three-dimensional model of the overlapped tunnel is established. The joints between the segments are represented by interface elements and joint bolts. The study is focused on the dynamic response of the tunnel lining, the internal force of segment lining, the opening and sliding of the interface between segments, and the mechanical properties of joint bolt and steel bar.

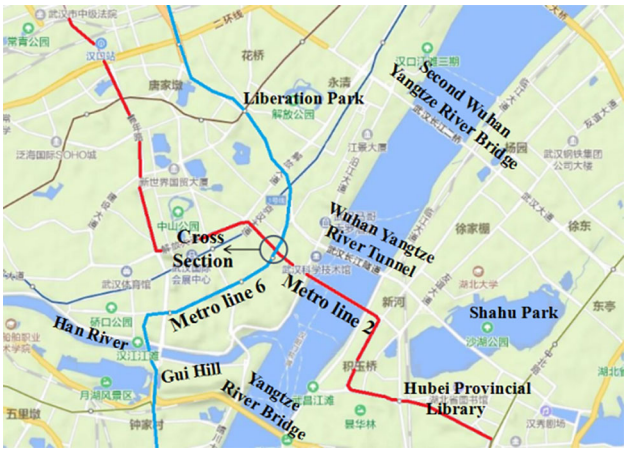

Fig. 1 Schematic diagram of overlapping of Metro Line 2 and Line 6 in Wuhan, China

2 Numerical Model

The overlapped tunnel section of Wuhan Metro Line 2 and Line 6 is mainly located in silty clay, which is considered as homogeneous soil layer in the following numerical modeling. Table 1 lists the soil parameters used in modeling. Metro Line 2 and Line 6 adopt the same cross-sectional circular lining with the inner diameter of 5.4 m and the outer diameter of 6.0 m. The lengths of Metro Line 2 and Line 6 are 80 and 100 m, respectively. The structure of the segment lining is shown in Fig. 2a. C50 reinforced concrete segments were used during the construction of Metro Line 2 and Line 6. The thickness and width of the linings are 0.3 and 1.5 m, respectively. The segment lining circumference adopts the '3 + 2 + 1' block method: 3 standard blocks (center angle is 67.5°), 2 adjacent blocks (center angle is 68.0°), and 1 capping block (center angle is 21.5°). The lining interface is connected with 16 longitudinal bending bolts and 12 circumference bending bolts. The bolt diameter is 27.0 mm, and the Poisson's ratio is 0.17. The finite element numerical model used in this study is shown in Fig. 2. Figure 2a shows the structure of the segment lining ring, Fig. 2b shows the whole model, Fig. 2c shows only the overlapped tunnels, and Fig. 2d illustrates the local fabricated segment linings of a shield tunnel.

The length and width of the model are 100.0, 80.0, and 60.0 m, respectively (Fig. 2b). The net vertical distance between the upper and lower tunnels is 2.0 m. The depth of the upper tunnel is 7.5 m. The segment linings are simulated by solid element (C3D8R) as shown in Fig. 2b. All the

Table 1 Physical and mechanical parameters

Material name	Density/(kg/m^3)	Elastic modulus/MPa	Poisson ratio	Friction angle (°)	Cohesion/ MPa
Soil layer	1900.0	50.0	0.35	22.0	0.03
Segment	2500.0	34,500.0	0.20	–	–
Ballast bed	2200.0	19,800.0	0.24	40	1.1
Rail	7800.0	210,000.0	0.17	–	–

boundaries except for the upper boundary are simulated using a continuously distributed parallel spring-damper system. According to Gu (2015) [18], the spring stiffness and damping coefficient in tangential and normal directions used in this study are determined as: 1.44×10^6 kN m, 2.85×10^6 kN m and 3.64×10^5 m/s, 7.78×10^5 m/s, respectively.

The surrounding soil layer and the ballast bed are also modeled by solid element (C3D8R). The Mohr–Coulomb elastic–plastic constitutive model is used for the surrounding soil layer and the ballast bed, whereas the elastic constitutive model is used for the segmental linings, track, and rail. The physical parameters of soil layer, segment, ballast bed, and rail are shown in Table 1.

2.1 Segment Lining

The subway shield tunnel is a prefabricated lining structure which is made up of fabricated segments connected by circumferential and longitudinal bolts (Fig. 2d). There are a lot of interfaces or joints between segment linings. Segment joints or interfaces are the weakest parts of the structure, which greatly affect the overall deformation of the tunnel. It is of great importance to properly simulate the joint behavior. The segment joint includes two components: lining concrete and joint bolt. In numerical modeling, these two components are modeled separately with the special focus on the joint effects and the interaction behavior between segments. In reality, the compressive and shear forces of the shield structure are mainly carried by the lining concrete, the tensile forces are mainly carried by the bolt, and the joint bending moment is carried by both lining concrete and bolts. The shield concrete and the joint bolt are simulated by the solid element (C3D8R). The two ends of the bolt are embedded in the lining concrete. The elastic modulus and the tensile strength of the bolt are 210.0 GPa and 800.0 MPa, respectively. The interaction between the segment linings are modeled by the interface elements. The interface and the joint are shown in Fig. 3.

Special attention should also be paid to the interaction between segment lining and the surrounding soil layer. This interaction is represented by the interface element. The normal contact of the interface element is 'hard contact,' which can transfer all kinds of interfacial pressure between the concrete and allow separation after contact, while the tangential contact is represented by the Coulomb friction model based on the penalty function, and the relative slip will remain still until the tangential stress reaches the predefined shear strength. The formula for the tangential contact is defined as: $\tau = \mu P$, where τ is the critical shear strength, μ is the friction coefficient, with the value of 0.70, and P is the normal contact pressure. The interaction between the track bed, the segment lining and the track is simply bound together by a 'tie' to simulate the overall forces and deformations.

Reinforcement (i.e., steel bars) of the segment linings is simulated by Truss elements. Steel bars are embedded in the segment concrete to simulate the reinforced concrete structure. Figure 4 shows an example of the reinforcement of the segment linings.

HPB300 (hot-rolled plain bar) with high strength and good plasticity is used as reinforcement in tunnel lining. The yield strength of the reinforcement is 300 MPa, the ultimate strength is 420 MPa, and both the designed tensile and compressive strength are 270 MPa. The outer bars include 8 steel bars of 22 mm diameter and 8 bars of 18 mm diameter. The inner steel bars include 16 bars of 32 mm diameter. The bar density is 7800.0 kg/m^3, the Poisson's ratio is 0.17, and the elastic modulus is 206.0 GPa. The Esmaeily model [19] is used to capture the yield, hardening, and softening behavior of steel bars. The model considers the yield point, hardening starting point, stress peak, and limit point of the steel bar, which is in good agreement with the material test results of steel bars. The constitutive relation of the Esmaeily model [19] is shown as follows:

$$\sigma_s(N) = \begin{cases} E_s\varepsilon_s, & \varepsilon_s \le \varepsilon_y \\ f_y(N), & \varepsilon_y < \varepsilon_s \le k_1\varepsilon_y \\ k_4 f_y(N) + \frac{E_s(1-k_4)}{\varepsilon_y(k_2-k_1)^2}(\varepsilon_s - k_2\varepsilon_y)^2, & \varepsilon_s > k_1\varepsilon_y \end{cases}, \tag{1}$$

where σ, ε are the stress and strain of steel bars, respectively; E_s is the elastic modulus of the steel bar; f_y and ε_y are the yield strength and yield strain of the steel, respectively; their values are determined as 300.0 MPa and 0.0015, respectively; k_1 is the ratio of the steel bar strain at the hardening starting point to the yield strain, and the value is 4.0; k_2 is the ratio of the peak strain to the yield strain of the steel bar, and the

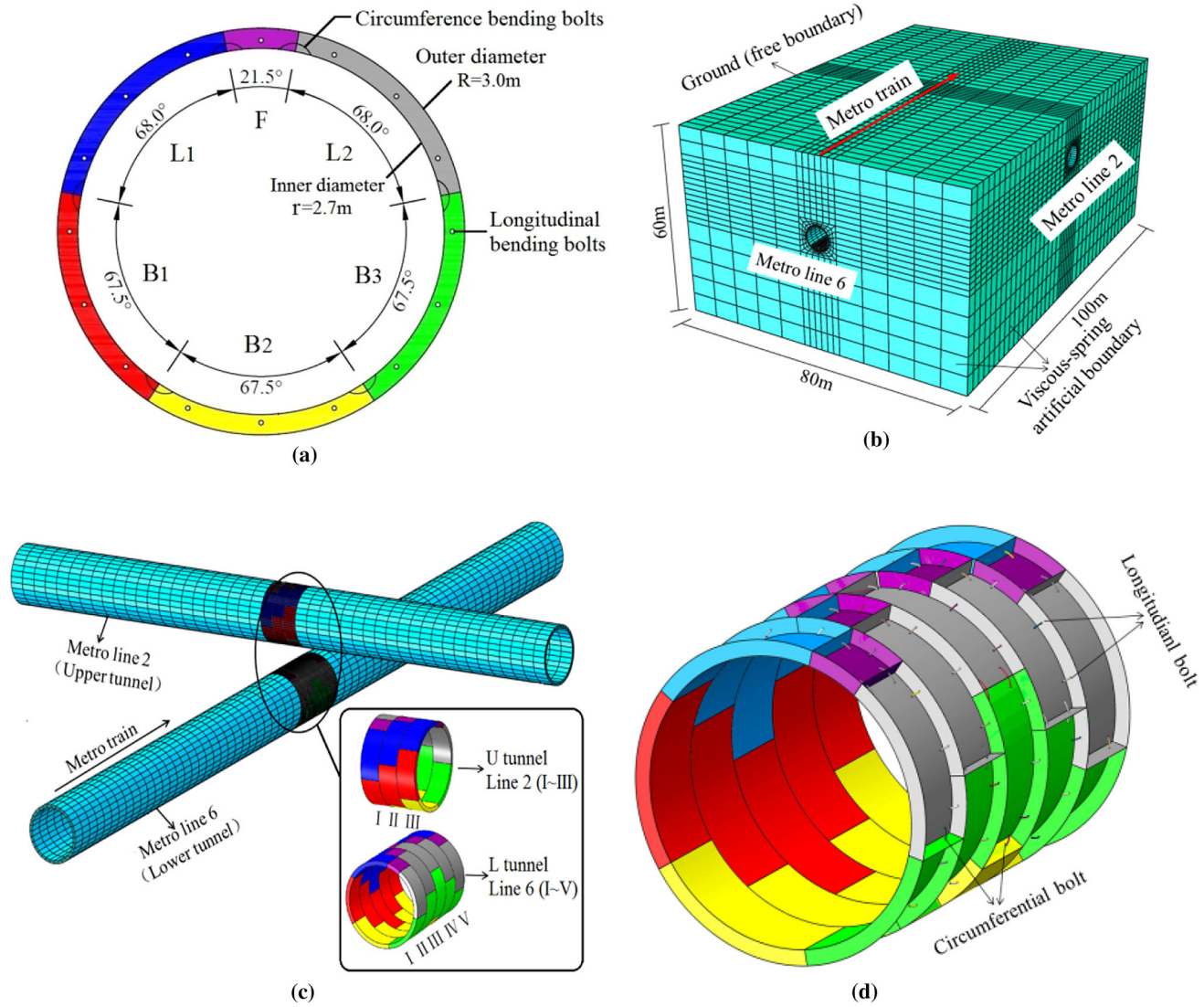

Fig. 2 Numerical model of the overlapped tunnels. **a** Structural map of the segment lining ring. **b** The whole model. **c** The overlapped model. **d** Local fabricated segment lining

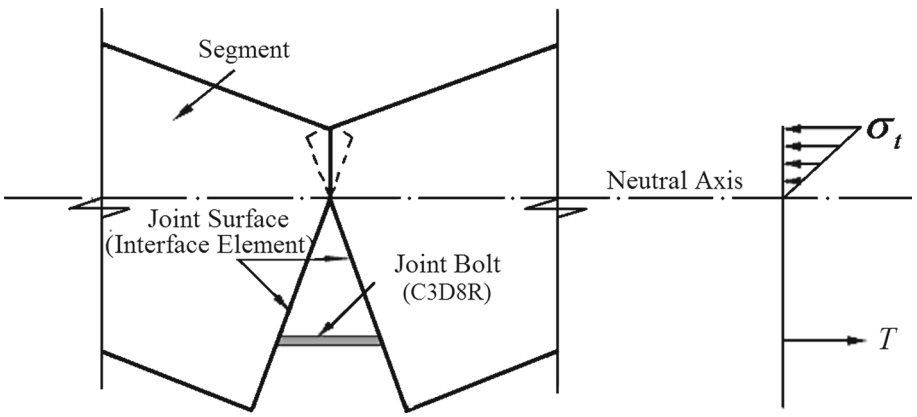

Fig. 3 Joint interface and joint bolt

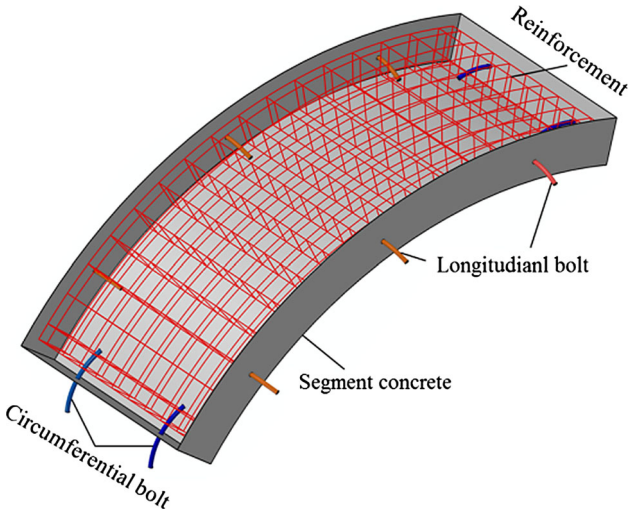

Fig. 4 Steel bars in adjacent block

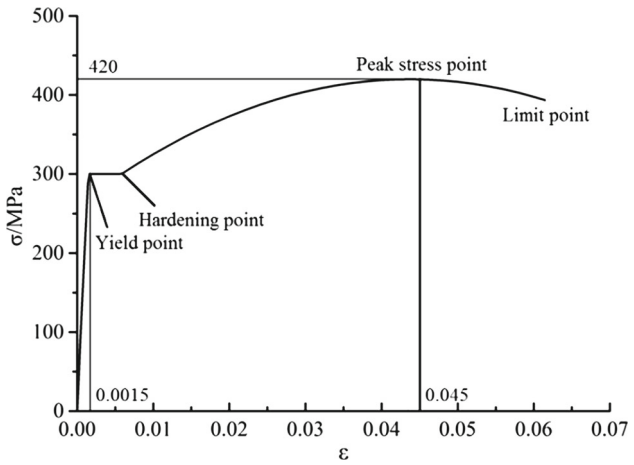

Fig. 5 HPB300 steel stress–strain relationship

value is 30.0; k_3 is the ratio of the peak stress and the yield strength of the steel bar, and the value is 1.4. Figure 5 shows the stress–strain relationship of the HPB300 steel bars.

2.2 Equivalent Stiffness of Tunnel Structure

The dynamic analysis requires high computational resources, especially when the joint interfaces are considered. Hence, only part of the tunnel is simulated by the fabricated segments and joint bolts, with the objective to improve the computational efficiency: only three circumference segments (I–III) in the middle of Line 2 (hereinafter referred to U tunnel) and five circumference segments (I–V) in the middle of Line 5 (hereinafter referred to as L tunnel) are modeled, as shown in Fig. 2b. The remaining segment linings of tunnel are modeled using the equivalent principle of flexural rigidity, where the joint effects are taken into account by reducing the overall bending rigidity of the structure. The equivalent bending stiffness equations are shown as follows [13]:

$$(EI)_{\mathrm{eq}} = \frac{\cos^3\varphi}{\cos\varphi + \left(\frac{\pi}{2} + \varphi\right)} E_{\mathrm{s}} I_{\mathrm{s}} \tag{2}$$

$$\varphi + \cot\varphi = \pi\left(0.5 + \frac{K_j}{E_{\mathrm{s}} A_{\mathrm{s}}/l_{\mathrm{s}}}\right), \tag{3}$$

where φ is the angle between the neutral axis and the horizontal line of the center of tunnel; E_{s} and A_{s} are lining elastic modulus and tunnel circumference section area, respectively; $A_{\mathrm{s}} = \pi(D^2 - d^2)/4$, D and d are the outer diameter and inner diameter of the shield tunnel, respectively. Moment of inertia of circle section$I_{\mathrm{s}} = \pi(D^4 - d^4)/64$; bolt tensile stiffness is the tensile stiffness of a single bolt, is the number of longitudinal bolts between circumferences, and is the lining circumference width. The equivalent flexural rigidity of tunnel lining is calculated as 4.3×10^7 kN m^2.

2.3 Soil Layer Damping

The damping used in this model is the Rayleigh damping, which is commonly used in dynamic analysis. The damping matrix is proportional to the mass and stiffness matrix, and its expression is:

$$[C] = \alpha[M] + \beta[K], \tag{4}$$

where $[M]$, $[C]$, and $[K]$ are the model's mass matrix, damping matrix, and stiffness matrix, respectively; α is the mass-dependent damping coefficient, and β is the stiffness-dependent damping coefficient. The relationship between the correlation coefficients and the damping ratio is satisfied:

$$\xi_k = \frac{\alpha}{2\omega_k} + \frac{\beta\omega_k}{2} \quad (k = 1, 2, 3 \ldots n), \tag{5}$$

where ξ_k is the damping ratio and ω_k is the free frequency. Two natural frequencies, ω_1 and ω_2, can be obtained by the frequency analysis of the model. Assume that the corresponding damping ratio are constants, i.e., $\xi_1 = \xi_2 = \xi = 0.05$; the coefficients α and β can be determined by:

$$\alpha = 0.05 \times \frac{2\omega_1\omega_2}{\omega_1 + \omega_2} \quad \beta = 0.05 \times \frac{2}{\omega_1 + \omega_2}. \tag{6}$$

The two natural frequencies, ω_1 and ω_2, can be determined by analyzing the frequency: $\omega_1 = 5.56\,\mathrm{rad}/s$ and $\omega_2 = 5.60\,\mathrm{rad/s}$. Hence, the coefficients α and β can be reached: $\alpha = 0.279$ and $\beta = 0.009$. According to formula (4), Rayleigh damping formula can be expressed as:

$$[C] = 0.279[M] + 0.0090[K]. \tag{7}$$

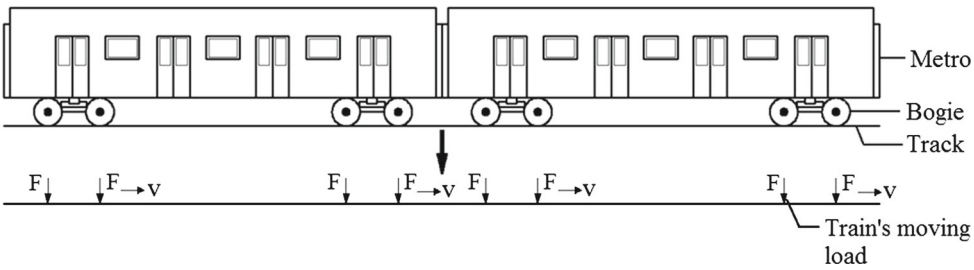

Fig. 6 Schematic diagram of relative position of moving loads on subway train

2.4 Train-Induced Vibration Loads

Wuhan Metro Line 2 and Line 6 trains are B-type vehicles, using 6 compartments marshaling. The length of each carriage is 19.0 m, the wheelbase is 2.2 m, the distance between the front and rear bogies is 12.6 m, and the standard gauge of 1435 mm is adopted. The designed maximum strain speed is 80 km/h. In this paper, the running speed of train is 72 km/h, and the train-induced loads which are moving with the train's movement are shown in Fig. 6.

Research shows that the main factors affecting the train-induced loads are the wheel–rail interaction and the dynamic effect. Currently, the train load time–history fitting formula is generally used in numerical modeling:

$$F(t) = P_0 + P_1 \sin \omega_1 t + P_2 \sin \omega_2 t + P_3 \sin \omega_3 t, \quad (8)$$

where P_0 is the wheel static load; P_1, P_2, and P_3 are vibration loads; the corresponding vibration load amplitude is expressed as follows:

$$P_i = M_0 \alpha_i \omega_i^2 \quad (i = 1, 2, 3), \quad (9)$$

where M_0 is the unsprung mass under the train; α_i is the typical vector height; ω_i is the circular frequency of the uneven vibration wavelength at the corresponding vehicle speed. The formula is:

$$\omega_i = \frac{2\pi v}{L_i} \quad (i = 1, 2, 3), \quad (10)$$

where v is the train running speed; L_i is a typical wavelength. In this paper, one side of the train static load is $P_0 = 80\,\text{kN}$ and the unsprung mass under the train is $M_0 = 750$ kg. The irregular vibration wavelength and the vector height are: $L_1 = 10.0$ m, $a_1 = 3.5$ mm; $L_2 = 2.0$ m, $a_2 = 0.4$ mm; $L_3 = 0.5$ m, $a_3 = 0.08$ mm, respectively. Figure 7 shows the time–history curve of train vibration load.

In the field, the train-induced vibration loads are transferred to the rail track by the wheel and are further distributed to the segment linings. In addition, the vibration loads applied to the segment linings vary with time. The influences of train operation on the adjacent overlapped tunnels are studied herein. The simulation only takes into account the case

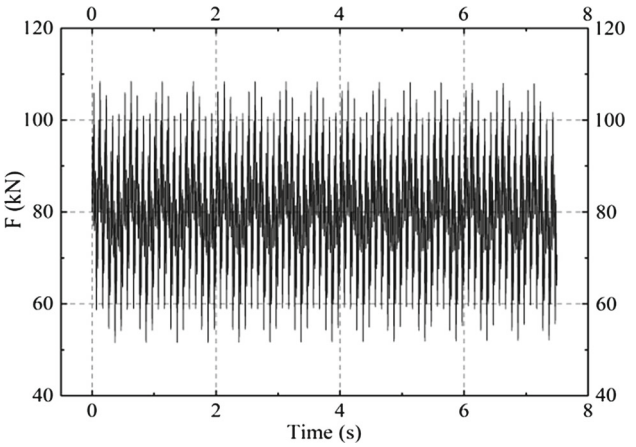

Fig. 7 Vertical vibration load curve of train (72 km/h)

of train running on the No. 6 line (the lower tunnel), with the aim to avoid the interference of trains running on the upper and lower at the same time. The direction of metro train operation is shown in Fig. 2a.

The shield tunnel contains fabricated segment linings with a large number of interfaces. Hence, the overall stiffness of the shield tunnel is relatively small, and the tunnel has poor stability. In order to facilitate the further discussions, tunnel segments are labeled by Greek letters I–V and joints are labeled by numbers ① ~ ⑥, which are shown in Fig. 8.

The segments of the overlapped section are labeled along the train driving direction. The segments of the upper tunnel are labeled by U-I to III, and the segments of the lower tunnel are labeled by L-I to V in turn. The joints or interfaces between segments are labeled by ① ~ ⑥ starting from the cap block counterclockwise. For example, U-II-1 represents the first interface or joint of the second segment of the upper tunnel.

3 Results Analysis

The dynamic response of overlapped tunnels under train vibration load is numerically studied, and the results interpretations are presented herein.

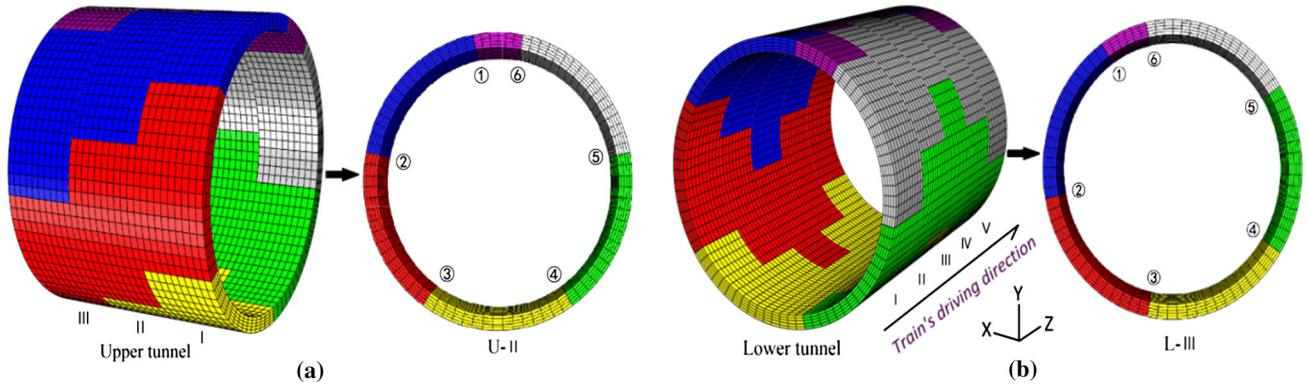

Fig. 8 Schematic diagram of segments and joint numbers. **a** Upper tunnel. **b** Lower tunnel

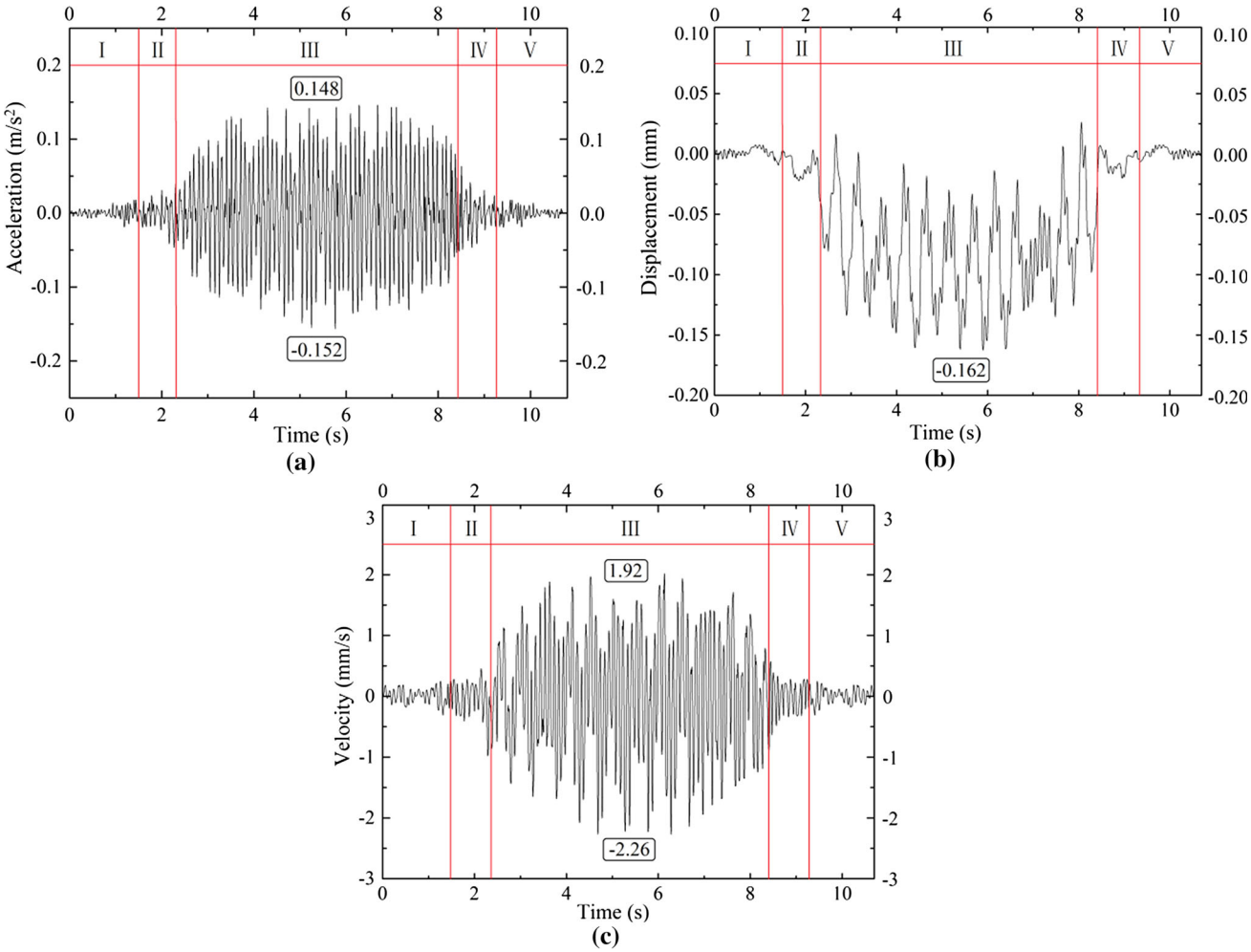

Fig. 9 Dynamic response time–history curves of midpoint of tunnel U-II section. **a** Acceleration. **b** Displacement. **c** Velocity

3.1 Dynamic Response Time–History of Segment Lining

The train operation mainly causes vertical vibrations, which are imposed on the tunnel linings. The dynamic response of the tunnel linings in terms of the vertical acceleration vs time curves, velocity vs time curves, and displacement vs time curves are obtained from the numerical simulation. Figure 9 shows the dynamic responses of the midpoint of the U-II segment, and Fig. 10 shows the dynamic responses of the midpoint of the L-III segment.

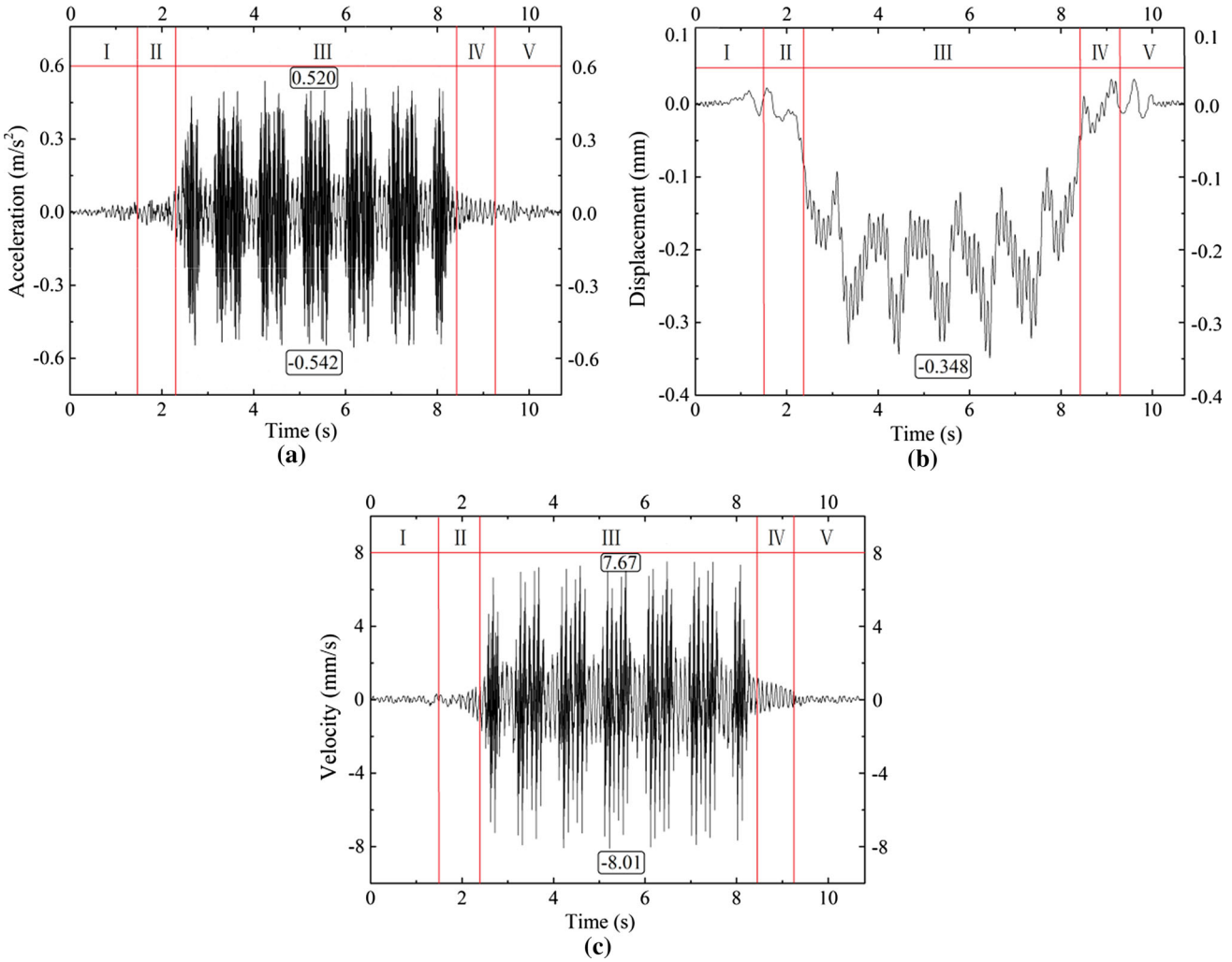

Fig. 10 Dynamic response time–history curves of midpoint of tunnel L-III section. **a** Acceleration. **b** Displacement. **c** Velocity

It takes 10.7 s for the train running through the overlapped upper (U tunnel in Fig. 8) and lower tunnel section (L tunnel in Fig. 8). The vibration response curve can be divided into five stages, based on the location of the train in the tunnel. When there is no train or the train is far away from the overlapped structure of the tunnel, the segment lining is in a relatively quiescent state, and the dynamic response values such as acceleration and velocity are smaller about zero.

The Stage A is the train approaching stage, with the train running time range of 0–1.5 s, during which the acceleration and velocity values almost remain at 0; the displacement shows a bit of fluctuation around 0 with the tendency to increase in the negative direction. The Stage B is the stage when a train reaches the overlapped tunnel section, with the time range of 1.5–2.3 s. The acceleration value, velocity, and displacement value increase gradually. The Stage C is the stage when the train passes through the overlapped tunnel section, and the time ranges from 2.3 s to 8.4 s. The acceleration and velocity values fluctuate greatly; the displacement gradually increases to the maximum value and fluctuates around that value. The Stage D is the stage when the train is leaving the overlapped section, with the time range of 8.4–9.2 s. The acceleration, velocity, and displacement values decrease gradually. The Stage E is the stage when the train runs away from the overlapped section. The acceleration, velocity, and displacement decrease toward zero as the train runs further away from the overlapped section.

The above analysis shows that the dynamic response of the segment linings is closely related to the relative location of the train. The train-induced vibration has greater influences on the lower tunnel than the upper tunnel as the train runs only in the lower tunnel. The maximum acceleration value (0.52 m/s^2) of the lower tunnel lining is only 10.4% of the structural safety control value (5.0 m/s^2) as specified in the research project during the train operation.

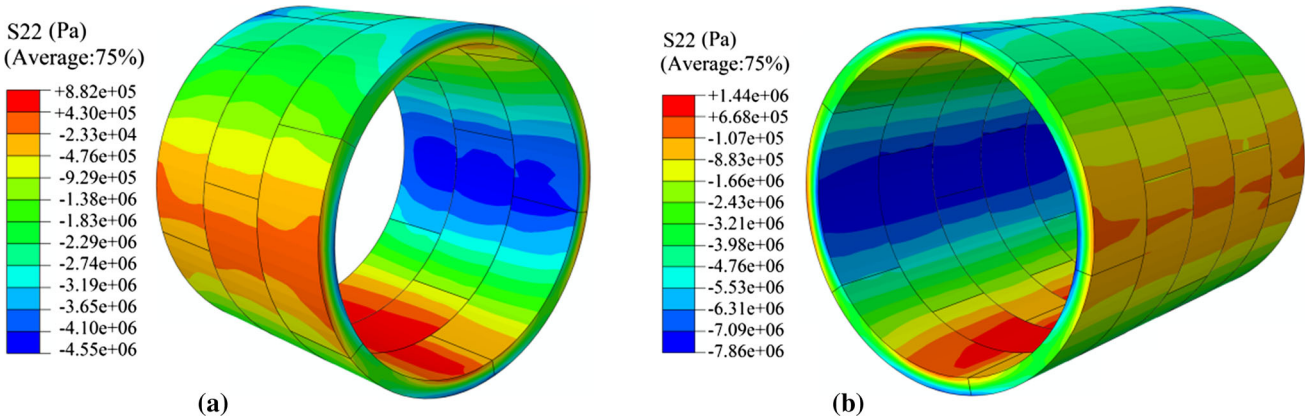

Fig. 11 Stress nephogram of overlapped tunnel segment circumference (Pa). **a** Upper tunnel. **b** Lower tunnel

3.2 Internal Forces of Segment Lining of Overlapped Sections

The stress distribution of the segment lining can be expressed by S22 stress. S22 stress is the circumferential stress under cylindrical coordinate, which reflects the state of tension–compression deformation at different positions of tunnel lining. Figure 11 shows the stress nephogram of the overlapped tunnel section when the train runs at 5.4 s.

As can be seen, U- II and L-III have similar stress distributions. At the arch top and arch bottom of the segment linings, the tensile stress is distributed inside of the segment linings, while the compressive stress is distributed outside of the segment linings. At both sides of the arch waist, the compressive stress is distributed inside of the segment linings, while tensile stress is distributed outside of the segment linings. It can be seen that the L-III segment lining has largest stresses, with the maximum compressive stress occurred inside of the arch bottom.

The segment linings are assumed to be in elastic stage. The axial stress and the bending moment of the overlapped section can be computed by integrating the stress of the segment:

$$N = \frac{1}{2}(\sigma_{\theta 1} + \sigma_{\theta 2})S \tag{11}$$

$$M = \frac{1}{2}(\sigma_{\theta 1} - \sigma_{\theta 2})\frac{I}{y}, \tag{12}$$

where N is axial force and M is the moment; $\sigma_{\theta 1}$ and $\sigma_{\theta 2}$ are the circumferential stresses of the inner and outer sides of the segment, respectively; S is the section area of the segment; I is the moment of inertia of the segment section about the longitudinal axis of the tunnel (Z axis); y is the distance between the center of the cross section and the distance from the outer edge.

The effects of joints on the internal force distributions are analyzed herein. Two numerical models are carried out: The first one uses the homogeneous ring equivalent stiffness model without consideration of joints; the second adopts the fabricated segment lining model with consideration of joints. The internal forces of U-II and L-III segments are plotted in Figs. 12 and 13 in the form of radar diagrams, respectively. The internal forces are extracted at every 9°, starting from the top arch of the tunnel and moving around the tunnel clockwise. These figures show the influences of joints on the internal force distributions of the overlapped tunnels under static loads. Static loads include vertical and horizontal earth pressure, water pressure, lining weight, foundation resistance, etc. The vertical load of the upper tunnel is calculated according to the actual overburden thickness, while the lower tunnel is calculated according to Terzaghi's vertical earth pressure formula. The lateral pressure coefficient of soil is 0.42, and the coefficient of formation elastic resistance is 25 MN/m^3.

As can be seen in Figs. 12 and 13, the internal force distributions of segment linings of overlapped tunnels under static load are similar. The segment linings are subjected to compressive axial forces. The top and bottom of the arch of the tunnel are subjected to positive bending moment, while the two sides of the arch waists are subjected to negative bending moment. The internal forces of the lower tunnel are larger than those of the upper tunnel due to the larger buried depth.

By comparing the stress distributions of lining with and without joints, it is found that the internal forces of the segment lining are relatively small when joints are taken into account. This shows that the overall stiffness of the segment is relatively small due to the existence of the longitudinal interface and the joint bolts.

The train vibration load will cause the additional internal forces on segment linings. Figures 14 and 15 show the radar diagrams of additional bending moment and peak axial forces caused by running trains.

It can be seen from Figs. 14 and 15 that the train-induced internal force distributions of the overlapped section are similar for the upper and lower tunnels. The L-segment is directly

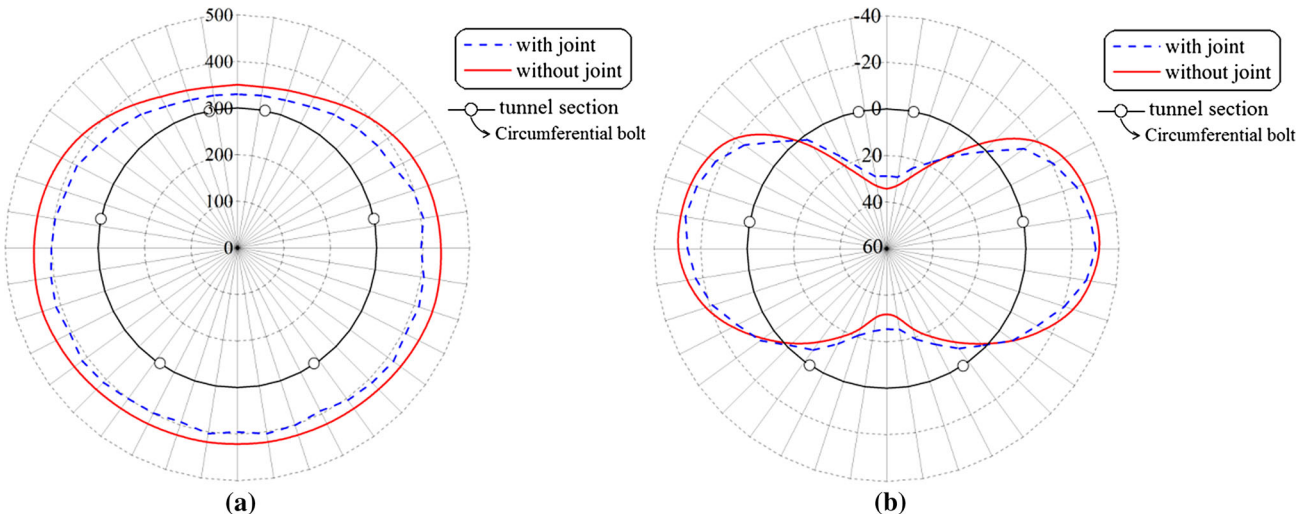

Fig. 12 Internal force distributions of U-II segment under the static load. **a** Axial force (kN). **b** Bending moment (kN m)

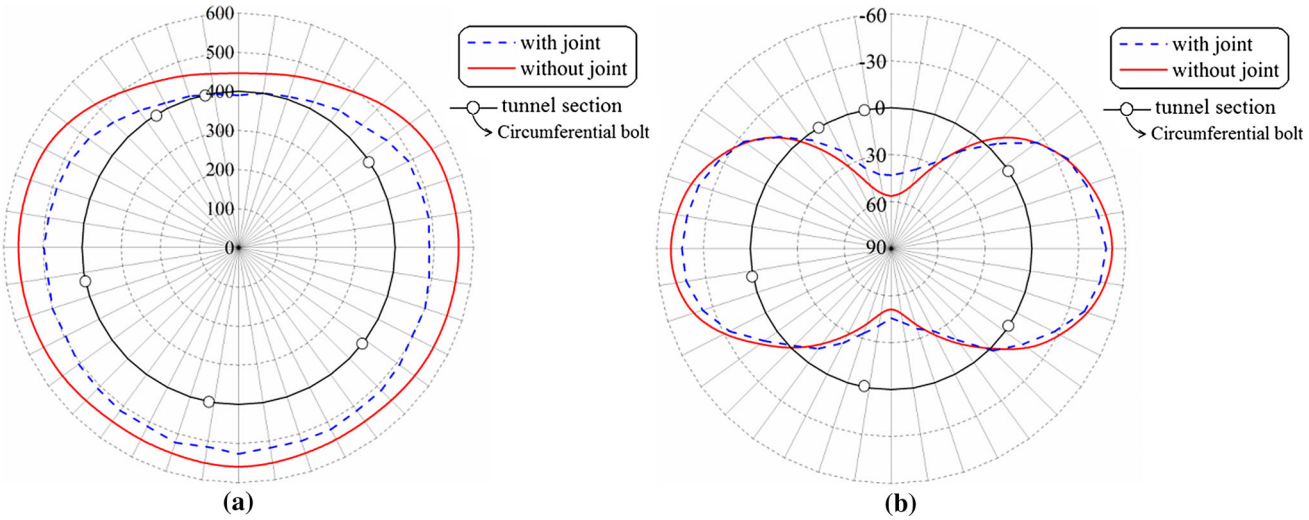

Fig. 13 Internal force distributions of L-III segment under the static load. **a** Axial force (kN). **b** Bending moment (kN m)

affected by the train vibration loads, and hence the additional internal forces are larger than those of U-segment.

When joints are taken into account, the axial force and bending moment of the segment vary at different positions. When joints are not considered, the overall axial force and bending moment are distributed smoothly and do not have abrupt changes. The internal forces of the segment with the consideration of joints are 2–3 times greater than the ones without joints.

The analysis shows that when lining joints are considered, the overall stiffness of tunnel is relatively small, and the internal force distribution varies greatly due to the influence of the interface and bolts. Therefore, the joint effects of lining structure should be considered in the future numerical analysis of shield tunnel.

3.3 Interface Opening and Stagger of Overlapped Section

The lower tunnel experiences larger deformation, as it is located in a deeper depth and is subjected to the direct dynamic loads caused by trains. The L-III-3 joint is chosen and studied with the purpose to analyze the opening and the staggered deformation of the segment linings of the lower tunnel. Figure 16 shows the vertical displacement and the joint deformation of the lower tunnel.

It can be seen from Fig. 16 that the joint deformation of the segment is large. Joints at the top and bottom of the arch have a tendency to open inward, while the joint at the arch waist tends to open outward. The contact state of the segment interface of L-III-3 joint is analyzed (Fig. 17). The tunnel inside is open (see the blue elements in the bottom right

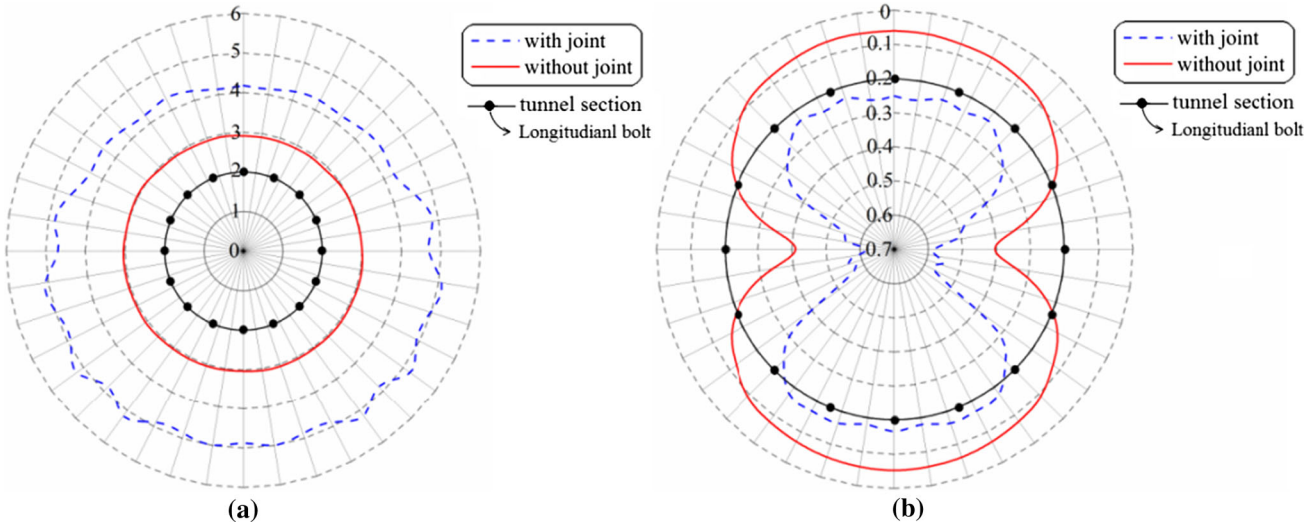

Fig. 14 Additional internal force distribution of U- II segment under train vibration load. **a** Additional axial force (kN). **b** Additional bending moment (kN m)

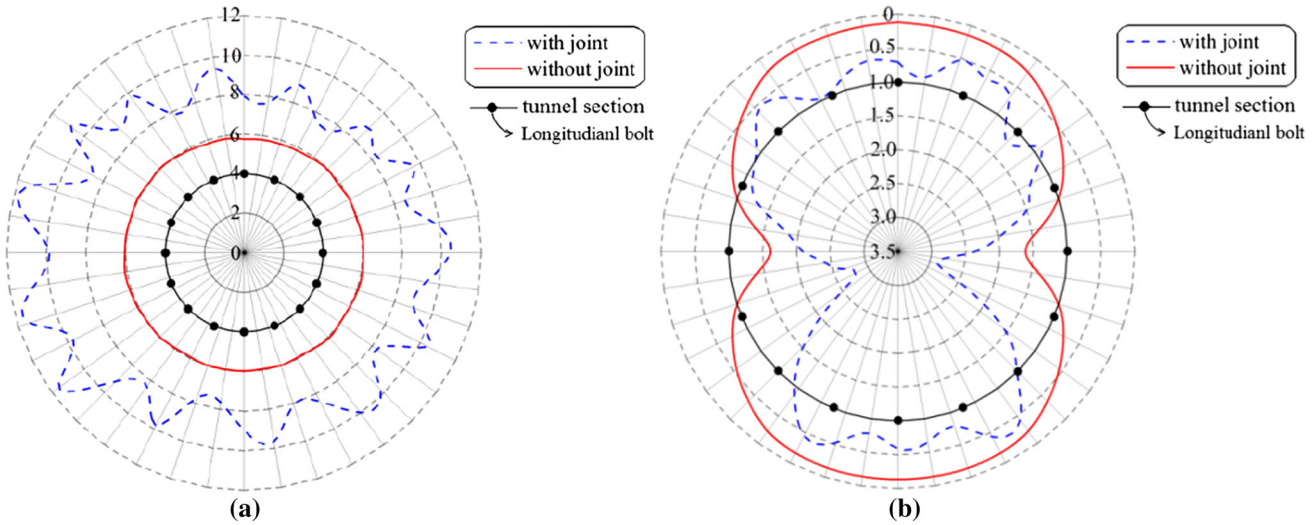

Fig. 15 Additional internal force distribution of L- III segment under train vibration load. **a** Additional axial force (kN). **b** Additional bending moment (kN m)

corner of Fig. 17), the contact pairs are separated, and the opened segment joint is shown in Fig. 17. The contact pairs are in bonding state at outside of the tunnel (the red elements in the bottom right corner of Fig. 17), and the segment joint is closed. The middle area is slipping (the green elements in the bottom right corner of Fig. 17), and the contact pairs have a tendency of separation and dislocation.

The segment linings experience the largest vibration in the C stage of lower tunnel (Fig. 10). The points I and O in Fig. 17 are selected as the monitoring points on the inner and outer edges of the interface. Figure 18 shows the time–history of the opening and staggered deformation.

From Fig. 18, the initial opening at I-point is about 0.314 mm. The opening increases due to the vibration loads, with the largest value reaching 0.321 mm. The net increase in the opening is 0.007 mm and hence. The opening deformation of the III-③ joint is small before the train operation reaches the III segment.

With the train operation, the III-③ joint opening increases quickly when the first set of bogie of the train reaches the III segment. The III-③ joint opening reduces to the initial value gradually when the bogie is leaving until the next set of bogie approaching. The joint opening effects exhibit partial superposition which is caused by interaction of two adjacent sets of bogies. The initial staggered value at point O is 0.053 mm. The presence of joints leads to inconsistent vibration responses at two adjacent segments, which induces the staggered deformation. The deformation of joints is associated with the train movement. In conclusion, the

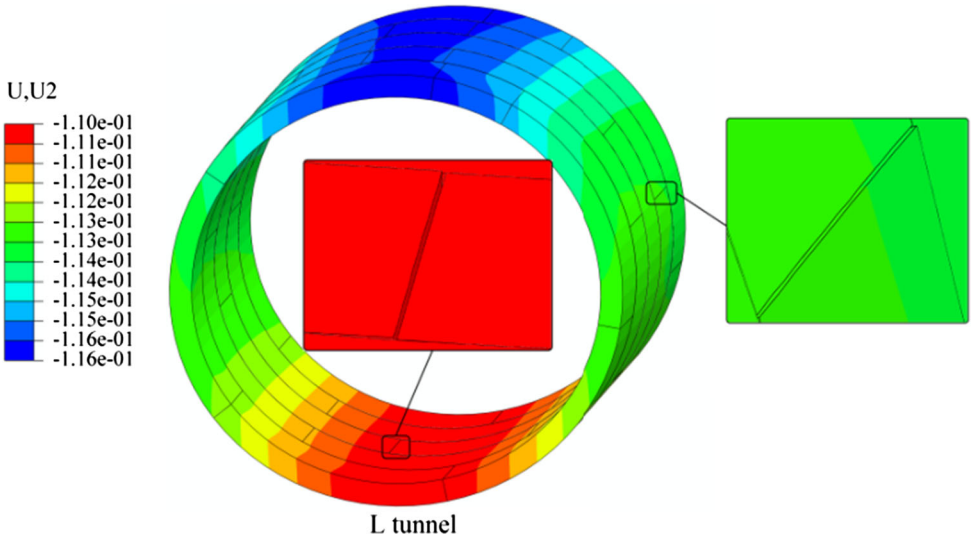

Fig. 16 Vertical displacement and joint deformation diagram of the lower tunnel (m/zoom 50 times)

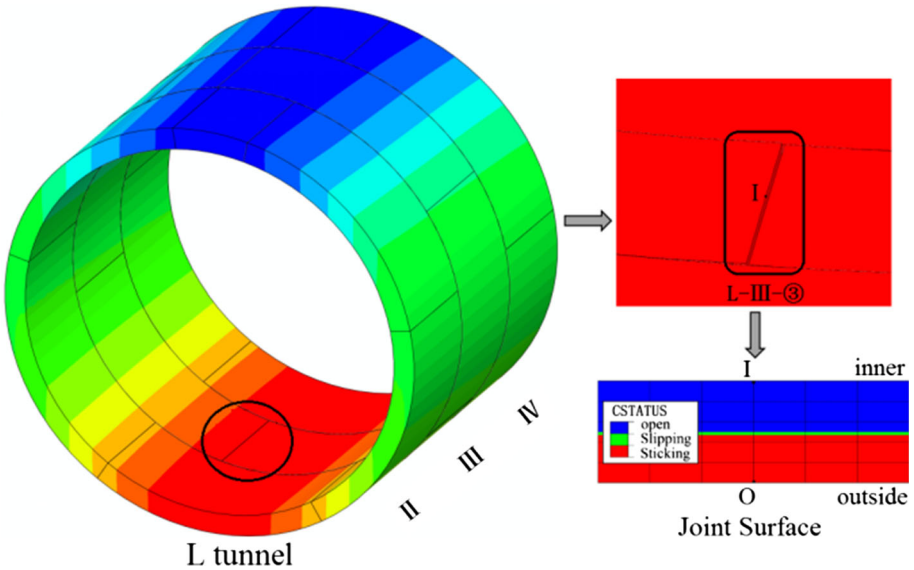

Fig. 17 Contact state of L-III-3 interface

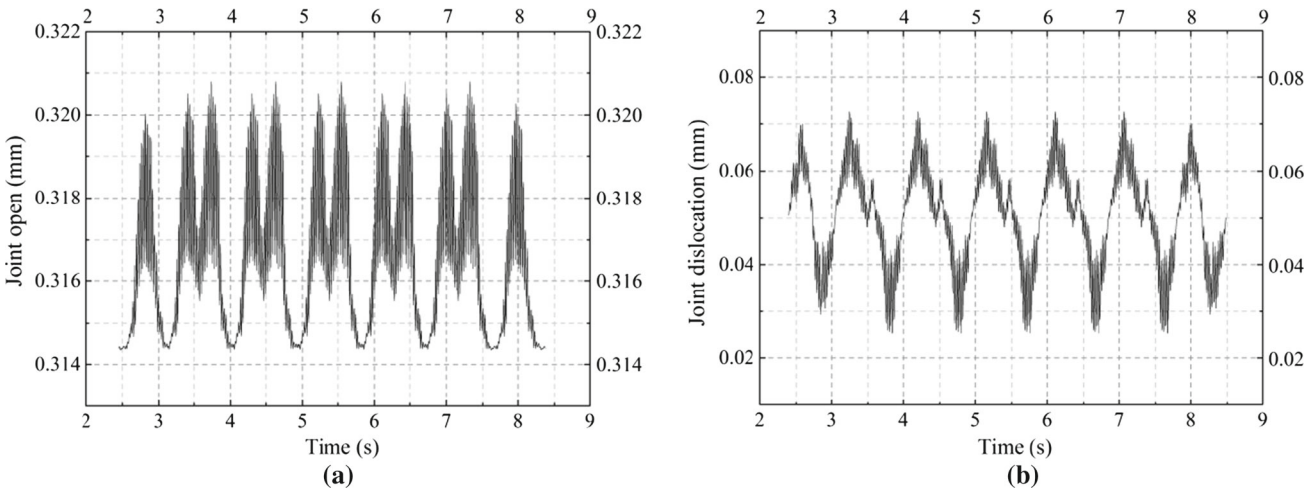

Fig. 18 Deformation time–history analysis of joint position point. **a** I-point opening time–history curve. **b** O-point displacement time–history curve

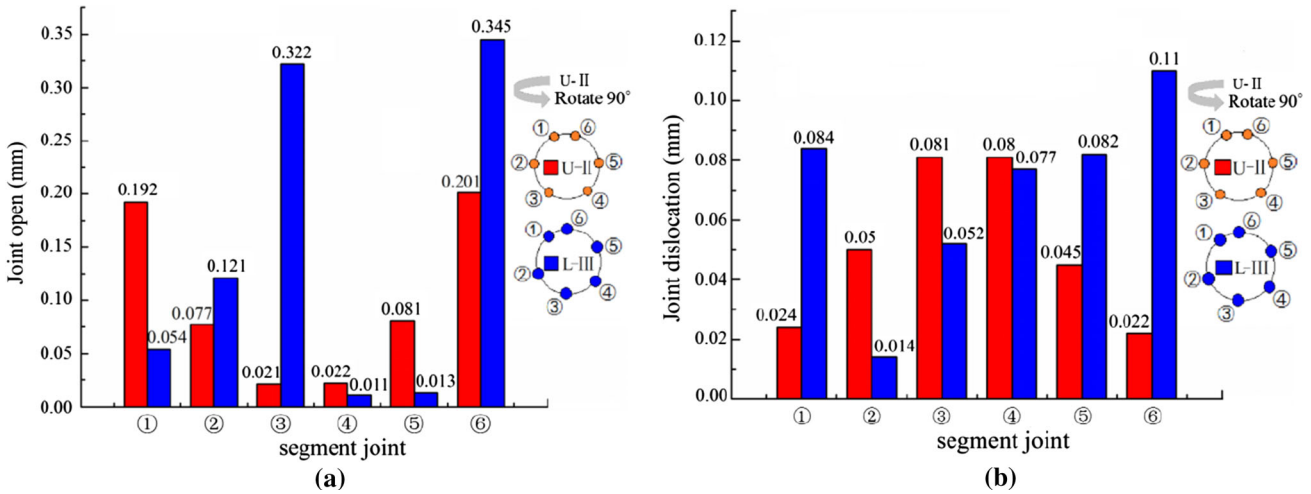

Fig. 19 Maximum deformation amount of segment joints. **a** Joint opening amount. **b** Joint dislocation amount

train-induced vibration loads influence the opening and staggered deformation of segment lining joint.

The maximum deformation of lining joints of U-II and L-III is extracted and shown in Fig. 19. Figure 19a, b shows the statistical columns of the maximum opening values and the dislocation values of the overlapped tunnel, respectively. The upper tunnel is rotated 90° counterclockwise to ease the interpretation. In Fig. 19, red columns refer to the deformation of U-II, while blue columns refer to the deformation of L-III.

It can be seen from Fig. 19 that the opening of U-II segment joints decreases gradually from the arch top to the arch bottom, with symmetrical distribution. The largest opening at the top of the arch is around 0.20 mm. However, the deformation of L-III segment joints varies greatly. The joint opening at the top and bottom of the arch is the largest, with the maximum opening value of 0.345 mm. The dislocation of U-II segment in Fig. 9b increases gradually from the top of the arch to the arch bottom, and the maximum dislocation is 0.081 mm. The dislocation at L-III is larger than that of U-II, and the maximum dislocation occurs at the top of the arch, i.e., the III-⑥ position.

The opening and dislocation deformations of L-III segment joints are relatively obvious, and the deformation varies at different joint locations. This indicates that in addition to the dynamic loads caused by the running trains, asymmetric distribution of the segment joint would affect the deformation of the segment. Hence, it is necessary to consider the segment lining joint distribution when performing numerical analysis.

3.4 Stress of Joint Bolts and Steel Bars of Segment Lining

The steel bar with the segment and the bolts at interface joint are subjected to train-induced dynamic loads. The joint bolts are numbered according to their location (Fig. 20). The joint positions were marked as B-II-① ∼ ⑥, B-III-① ∼ ⑥, which are shown in Fig. 20. For instance, B-II-① indicates the connecting bolts at the first joint position of the second circumference segment of the upper tunnel.

The stress distribution in the reinforcement of segment can be expressed by Mises stress. Mises stress is a comprehensive index to judge whether a material enters plasticity when the reinforcement is in a complex stress state. Through its distribution, the material forming state can be judged. Figure 21 shows the Mises stress of the steel bars of overlapped tunnel when the train is at 5.4 s. It can be seen from Fig. 21 that the stress distribution of steel bars of overlapped tunnels U-II, L-III are basically the same. The steel bars have larger stresses when the corresponding segment has larger deformation. The maximum stress of L-III steel bars is 59.1 MPa, which is larger than the maximum value of 34.7 MPa for U-II steel bars. The maximum stress value of 59.1 MPa does not exceed the yield strength of steel bar, implying that the built-in steel bars are in elastic stage and not damaged by the dynamic loads.

Joint opening and staggered deformation can cause additional internal force of joint bolts. Figures 22 and 23 show the principal stress and internal forces of bolts of U-II and L-III segment, respectively.

The additional principal stress, the additional axial force, and the additional shear force of the circumferential bolts were extracted and analyzed, as shown in Figs. 22 and 23. The additional axial force and the additional shear force of the bolts in the figure refer to the average value of the internal forces of the two bolts in each circumference interface.

Figure 22 shows the additional principal stress time–history curve of the overlapped tunnel. The main stress of the joint bolts in the lower tunnel is larger than that of the upper tunnel bolts. This is due to the fact that the lower tun-

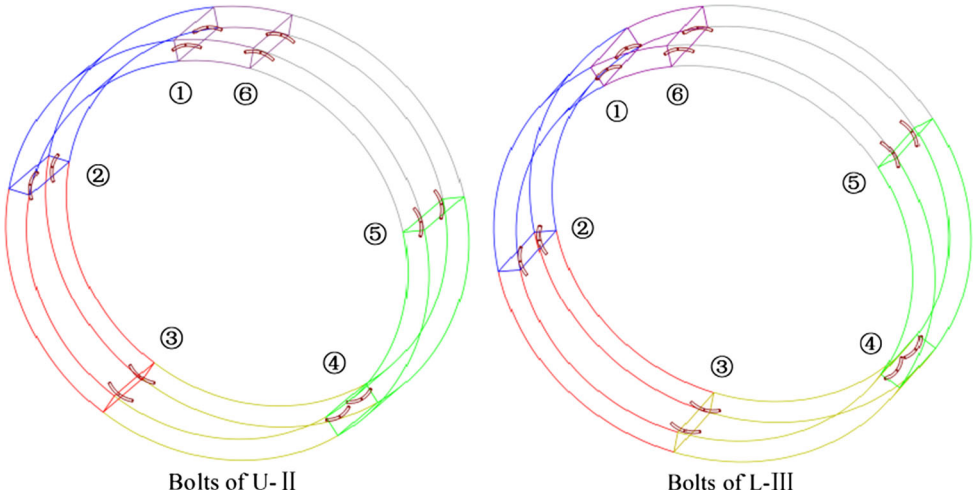

Fig. 20 Joint bolt locations in upper and lower tunnels. **a** Upper tunnel. **b** Lower tunnel

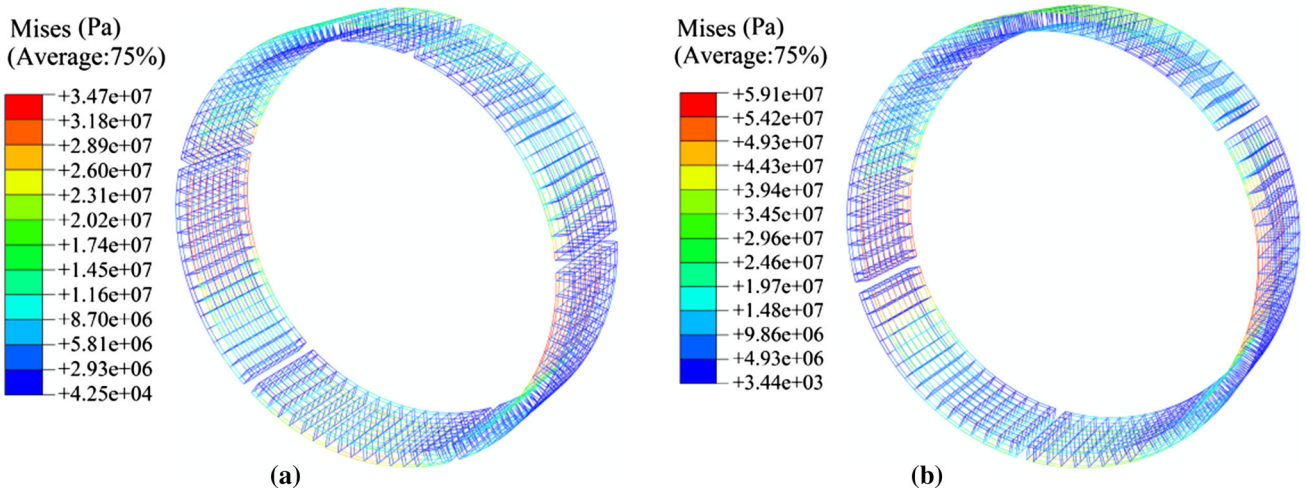

Fig. 21 Stress nephogram of segment lining bars. **a** U-II lining circumference steel bar. **b** L-III lining circumference steel bar

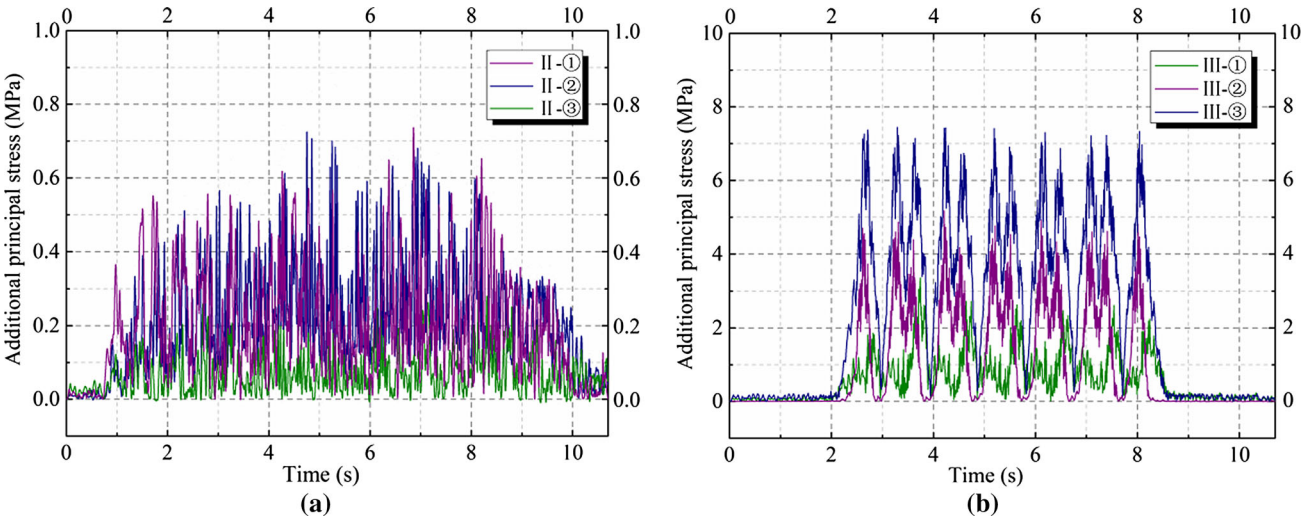

Fig. 22 Bolt additional principal stress response. **a** B-II. **b** B-III

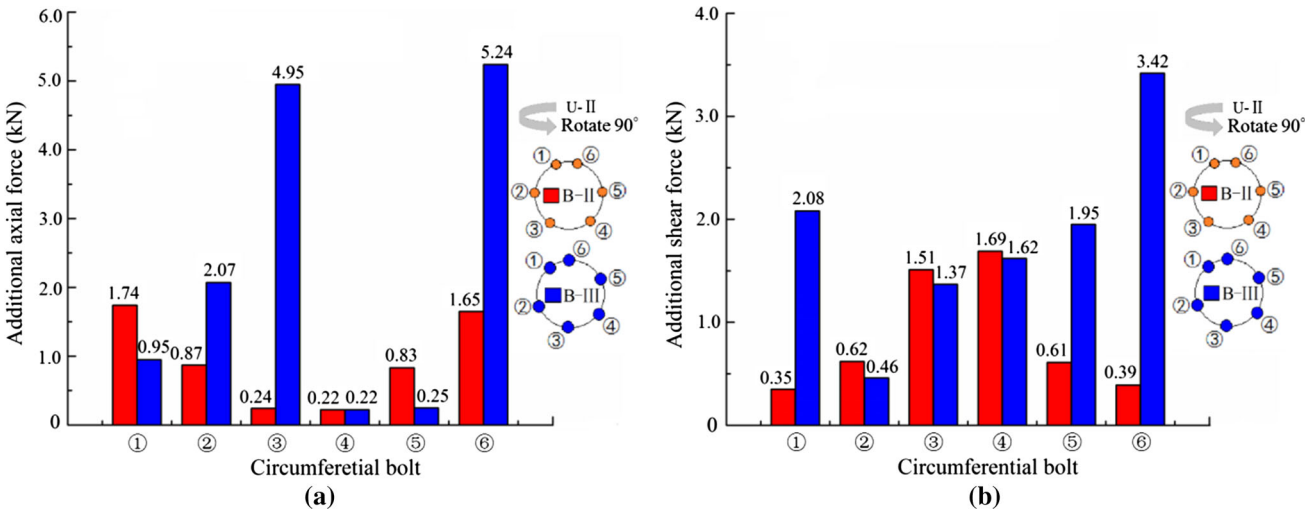

Fig. 23 Maximum value of additional internal force of typical bolts. **a** Additional axial force (kN). **b** Additional shear force (kN)

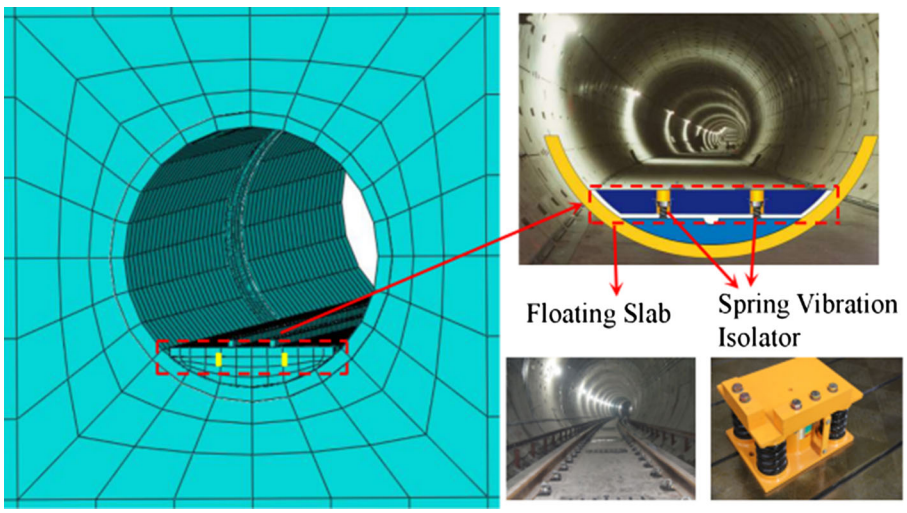

Fig. 24 Floating slab track system and the model

nel is directly affected by the train-induced dynamic loads. The upper tunnel is subjected to vibration waves which are reduced during their propagation in the rock mass to the upper tunnel.

It can be seen from Fig. 23 that the internal forces of joint bolts are associated with the joint deformation. The additional axial forces and shear forces are larger when a joint has larger opening and staggered deformation. The maximum additional axial force and shear force of L-III segment joint bolts are 5.24 and 3.42 kN, respectively, which are located in the top of the arch.

3.5 Damping Effect of the Spring Floating Slab Track System

The damping effects of the floating slab track system (FSTS) on the vibration of the train were also studied herein. The tunnel dynamic response analysis of the floating slab track system was carried out. The floating slab track system is a vibration damping structure which supports the track with an elastic isolator on the invert of the tunnel, and makes the track floating on the foundation structure, with a good damping effect. The floating slab track system was numerically represented by the floating slab and spring vibration isolator. The elastic modulus of floating slab is 35.0 GPa, and the density is 2500 kg/m. The stiffness of spring vibration isolator is 6.0 Pa/m, and the damping is 10.0 kN s/m. The layout of the floating slab track system is shown in Fig. 24.

The dynamic responses of the vertical acceleration, velocity, and displacement of the midpoint of the L-III segment in the lower tunnel under train-induced dynamic loads after adopting the steel spring floating slab track were calculated. Comparison between the vertical acceleration of midpoint of the L-III segment before and after application of the FSTS system is shown in Fig. 25a, the comparison of the displace-

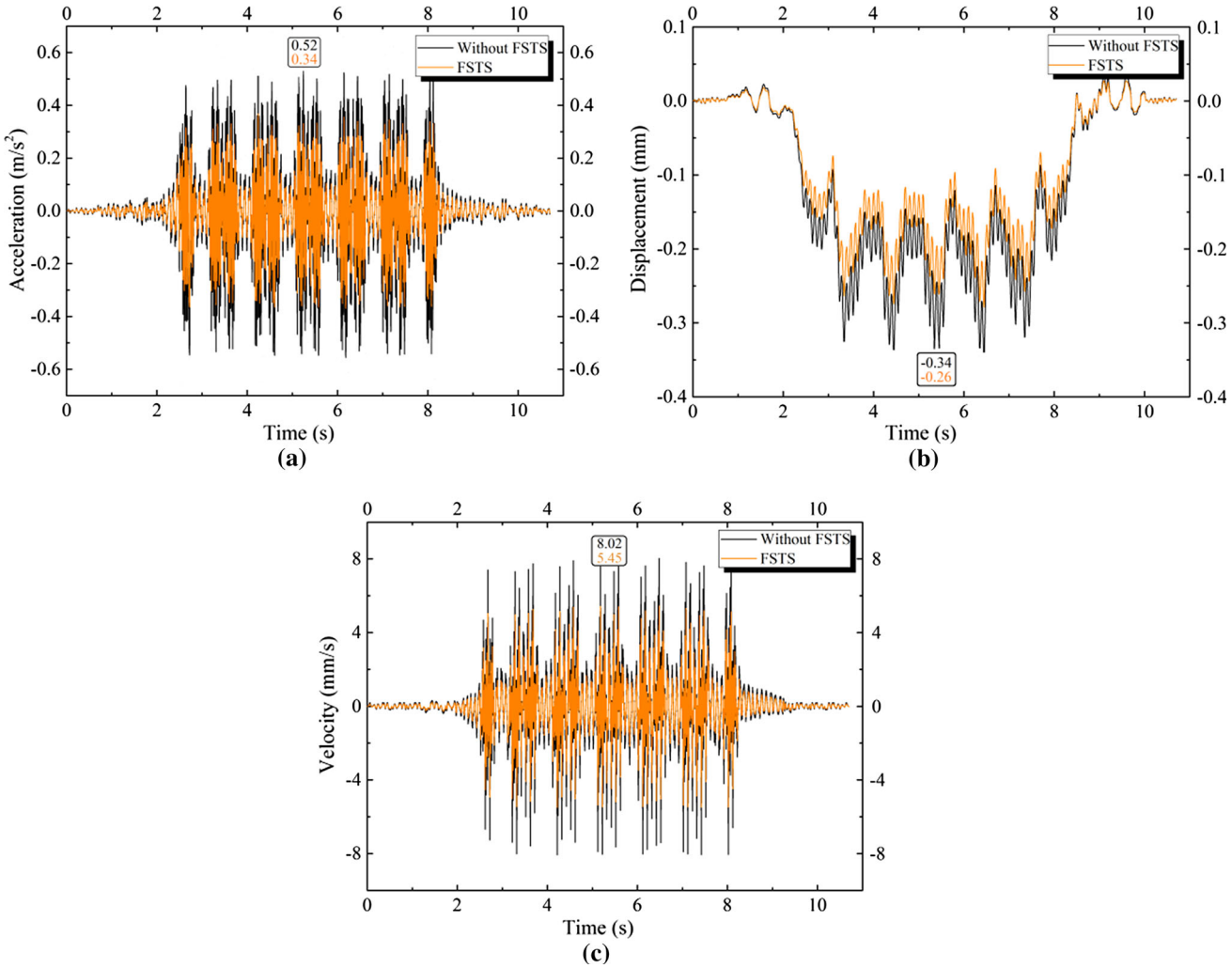

Fig. 25 Dynamic responses of the vertical acceleration, velocity, and displacement of the midpoint of the L-III segment before and after application of the FSTS system. **a** Acceleration. **b** Displacement. **c** Velocity

ment is shown in Fig. 25b, and the comparison of the velocity is shown in Fig. 25c.

It can be seen from Fig. 25 that the dynamic responses of the midpoint of the L-III segment are greatly reduced after the application of the FSTS system. The dynamic response of the tunnel linings in terms of the vertical acceleration vs time curves, velocity vs time curves, and displacement vs time curves with the FSTS system is similar to the curves without the FSTS system. But the maximum value of the vertical acceleration, velocity, and the displacement at the arch bottom of the lower tunnel is 0.65 times, 0.68 times, and 0.76 times of the tunnels without the FSTS system. By comparing the time history of acceleration and velocity, floating slab track system can effectively reduce vibration. Therefore, FSTS has become a widely used seismic mitigation measure in practical engineering.

4 Conclusion

The dynamic response of the overlapped section of the Wuhan Metro Line 2 and Line 6 shield tunnels is numerically studied herein. Joint interfaces between segment linings are explicitly modeled in the numerical simulation, and mechanical properties of steel bars and joints are properly accounted for. The findings are shown as follows:

1. The dynamic response of the overlapped tunnels is affected by the train-induced variation. The dynamic response can be divided into five stages due to the location of a train. The tunnel where a train is running has larger vibration loads, whereas the overlapped adjacent tunnel has less dynamic effects from the train. Two sets of bogies will cause superposition of vibration loads.
2. The additional internal forces of segment linings under the train-induced dynamic loads are affected by joint

interfaces and joint bolts. Hence, there is a need to take into account joint interface and bolts when analyzing the dynamic responses of shield tunnels.

3. The opening and staggered deformation occurs at joints of segment linings as the train is running through the overlapped tunnels. Joints open inward at the top and bottom of the arch, whereas joints open outward at the waist of the arch. The joint deformation is associated with the train locations.
4. The stress of steel bars under the vibration loads of subway trains is smaller than the yield strength. The steel bars are elastic and do not yield due to the train-induced vibrations. The internal forces of joint bolts are associated with the joint deformation. The internal force of joint bolts is larger, when the deformation of the joint where bolts are installed is larger.
5. The floating slab track system can greatly reduce the vertical acceleration and the displacement at the arch bottom of the lower tunnel, due to the damping cushioning effect of the floating slab track system. Under train-induced dynamic loads, the vertical acceleration and the displacement at the arch bottom of the lower tunnel were 0.65 times and 0.78 times of the tunnels without the FSTS system.

In this study, only the case of train running in the lower tunnel is considered, which aims to more clearly reveal the influences of trains on adjacent tunnel. The further study will focus on the dynamic response of tunnels caused by trains simultaneously running in the upper and lower tunnels.

Acknowledgements Financial support for this work provided by the National Key R&D Program of China (Grant No. 2016YFC0802205), and the National Science Foundation of China (Grant Nos. 51278425 and 51678500) is gratefully acknowledged.

References

1. Yamaguchi, I.; Yamazaki, I.; Kiritani, Y.: Study of ground-tunnel interactions of four shield tunnels driven in close proximity, in relation to design and construction of parallel shield tunnels. Tunn. Undergr. Space Technol. **13**(3), 289–304 (1998)
2. Liu, Z.; Wang, Y.; Liang, J.: Dynamic interaction of twin vertically overlapping lined tunnels in an elastic half space subjected to incident plane waves. Earthq. Sci. **29**(3), 185–201 (2016)
3. Gupta, S.; Berghe, H.V.D.; Lombaert, G.; et al.: Numerical modelling of vibrations from a Thalys high speed train in the Groene Hart tunnel. Soil Dyn. Earthq. Eng. **30**(3), 82–97 (2010)
4. Chen, W.Z.; Zhang, D.; Yu, J.X.: Study on stability of close cross tunnel on existing tunnel. Chin. J. Rock Mech. Eng. **34**(S1), 3097–3105 (2015)
5. Lai, J.; Wang, K.; Qiu, J.; et al.: Vibration response characteristics of the cross tunnel structure. Shock Vib. **2016**, 1–16 (2016)
6. Clot, A.; Arcos, R.; Romeu, J.; et al.: Dynamic response of a double-deck circular tunnel embedded in a full-space. Tunn. Undergr. Space Technol. **59**(1), 146–156 (2016)
7. Xue, F.: Dynamic responses of subway tunnel in clay stratum to moving loads. Arab. J. Sci. Eng. **42**(3), 1–14 (2017)
8. Gardien, W.; Stuit, H.G.: Modelling of soil vibrations from railway tunnels. J. Sound Vib. **86**(7), 605–619 (2003)
9. Yan, Q.; Chen, C.; Huang, X.; et al.: Analysis on vibration response characteristics of cross structure between shield tunnels and cross passage induced by the train. China Civ. Eng. J. **48**(S1), 228–235 (2015)
10. Real, T.; Zamorano, C.; Ribes, F.; et al.: Train-induced vibration prediction in tunnels using 2D and 3D FEM models in time domain. Tunn. Undergr. Space Technol. **49**, 376–383 (2015)
11. Gharehdash, S.; Barzegar, M.: Numerical modeling of the dynamic behaviour of tunnel lining in shield tunneling. KSCE J. Civ. Eng. **19**(6), 1626–1636 (2015)
12. Li, Z.; Soga, K.; Wang, F.; et al.: Behaviour of cast-iron tunnel segmental joint from the 3D FE analyses and development of a new bolt-spring model. Tunn. Undergr. Space Technol. Inc. Trenchless Technol. Res. **41**(1), 176–192 (2014)
13. Yan, Q.X.; Liu, J.; He, C.; et al.: The application of reaction displacement method in seismic analysis of shield tunnel. Railw. Eng. **50**(1), 77–80 (2010)
14. Hefny, A.M.; Chua, H.C.: An investigation into the behaviour of jointed tunnel lining. Tunn. Undergr. Space Technol. Inc. Trenchless Technol. Res. **21**(3), 428–428 (2006)
15. Deng, F.H.; Mo, H.H.; Zeng, Q.J.; et al.: Analysis of the dynamic response of a shield tunnel in soft soil under a metro-train vibrating load. Int. J. Min. Sci. Technol. **16**(4), 509–513 (2006)
16. Mo, H.H.; Deng, F.; Wang, J.: Analysis of dynamic responses of shield tunnel during metro operation. Chin. J. Rock Mech. Eng. **25**, 3507–3512 (2006)
17. ABAQUS Inc. Abaqus theory manual, Providence: ABAQUS Inc. USA (2007)
18. Gu, Y.: Theoretical Analysis of the Efficient Numerical Method for Soil-Structure Dynamic Interaction and its Application. Tsinghua University, Beijing (2005)
19. Esmaeily, A.: Behavior of reinforced concrete columns under variable axial loads. ACI Mater. J. **101**(1), 124–132 (2005)